

## **Supporting Information**

### **Amplification of Oxidative Stress by Lipid Surface-Coated Single-Atom Au Nanozymes for Oral Cancer Photodynamic Therapy**

Ming-Hsien Chan<sup>a,b,c,†</sup>, Bo-Gu Chen<sup>a,†</sup>, Chien-Hsiu Li<sup>b</sup>, Wen-Tse Huang<sup>a</sup>, Ting-Yi Su<sup>a</sup>,  
Lichang Yin<sup>d,\*</sup>, Michael Hsiao<sup>b,e,\*</sup>, and Ru-Shi Liu<sup>a,\*</sup>

<sup>a</sup> *Department of Chemistry, National Taiwan University, Taipei 10617, Taiwan*

<sup>b</sup> *Genomics Research Center, Academia Sinica, Taipei 11529, Taiwan*

<sup>c</sup> *Department of Biomedical Imaging and Radiological Science, National Yang Ming  
Chiao Tung University, 11221, Taipei, Taiwan*

<sup>d</sup> *Shenyang National Laboratory for Materials Science, Institute of Metal Research,  
Chinese Academy of Sciences, Shenyang 110016, China*

<sup>e</sup> *Department and Graduate Institute of Veterinary Medicine, School of Veterinary  
Medicine, National Taiwan University, 10617, Taipei, Taiwan*

† These authors contributed equally.

\* Corresponding authors

Correspondence and requests for materials should be addressed to Ru-Shi Liu (email:  
[rsliu@ntu.edu.tw](mailto:rsliu@ntu.edu.tw)), or Michael Hsiao (email: [mhsiao@gate.sinica.edu.tw](mailto:mhsiao@gate.sinica.edu.tw)), or Lichang  
Yin ([lcyin@imr.ac.cn](mailto:lcyin@imr.ac.cn)).

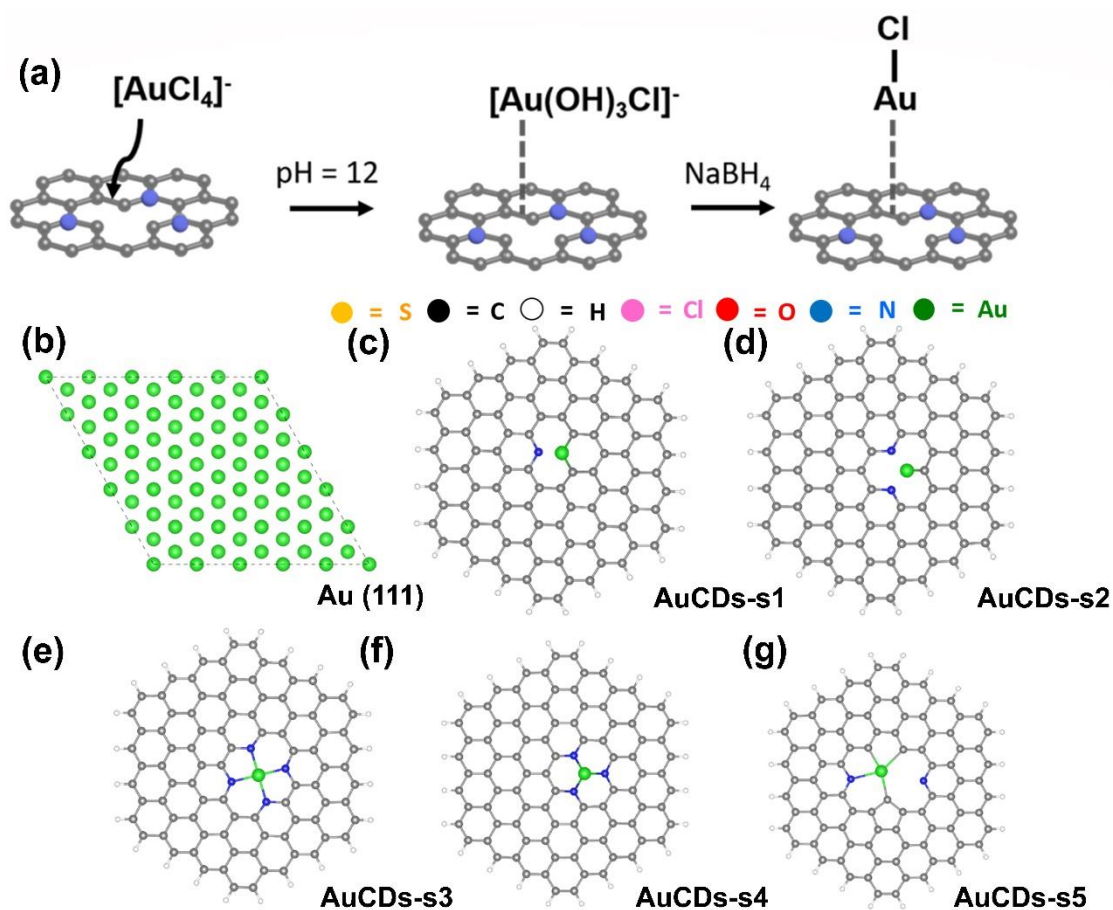


**Fig. S1.** Theoretical calculations are performed to investigate the possible coordination of single-atom gold in the structural defects of the carbon quantum dot. (a) The formation mechanism of AuCDs is proposed. (b-g) The probable forms of AuCDs.

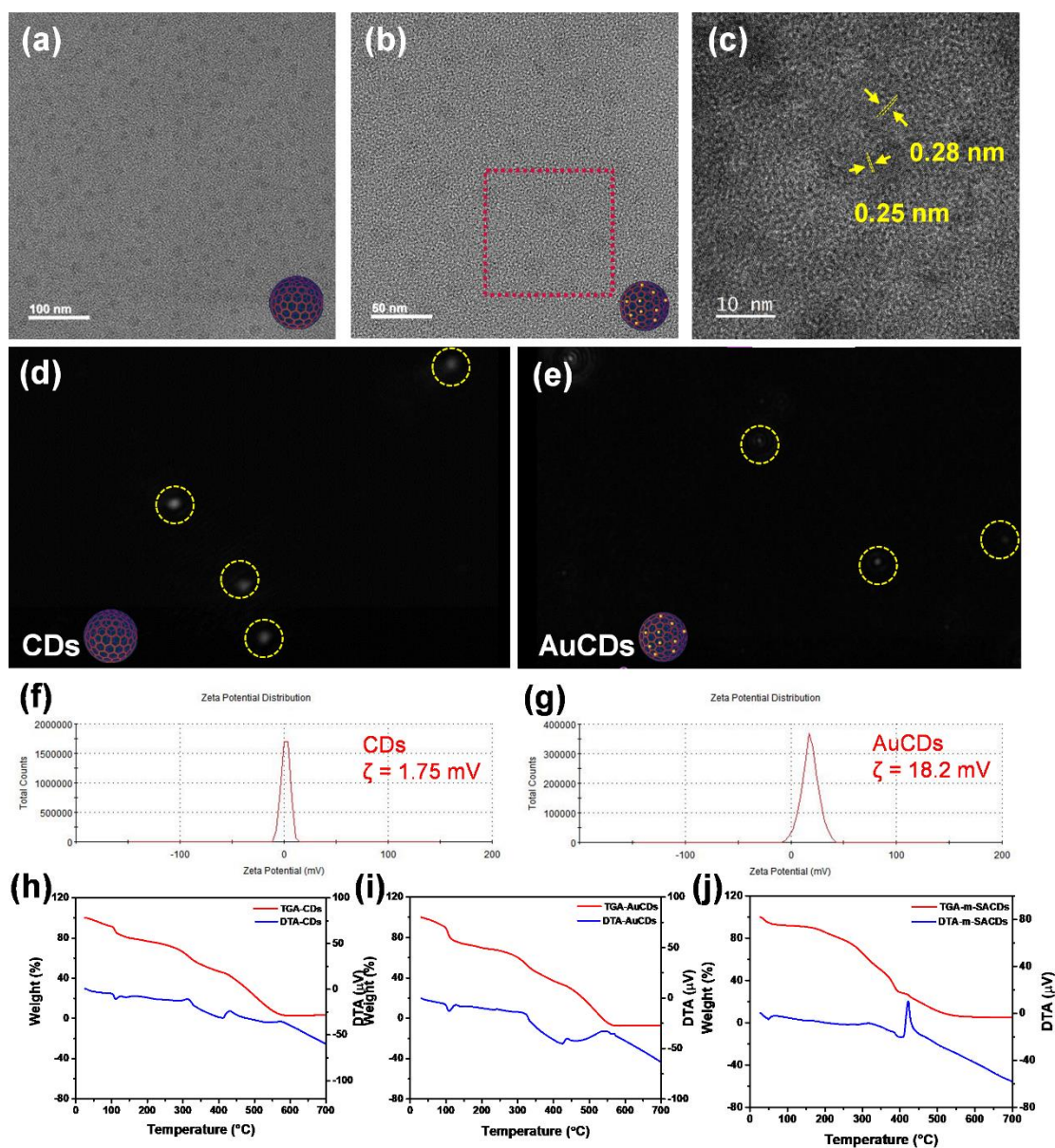


**Fig. S2.** Other physical characterization tests were performed for both the CDs and AuCDs groups. Large-scale TEM image analysis of (a) CDs and (b) AuCDs. (c) TEM image of AuCDs zoomed in to view the lattice structure. NTA results of (d) CDs and (e) AuCDs. Zeta potential results of (f) CDs and (g) AuCDs. TGA-DTA results of (h) CDs, (i) AuCDs, and (j) m-SACDs.

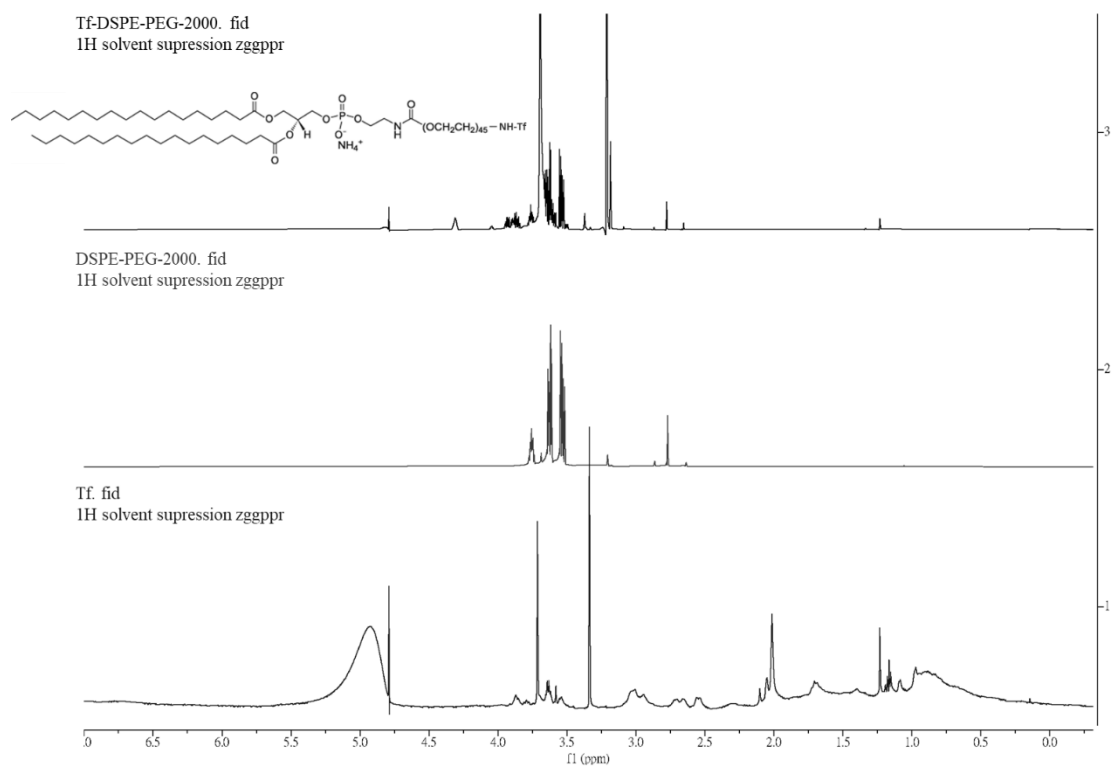


**Fig. S3.** The  $^1\text{H}$ -NMR spectra of Tf-DSPE-PEG-2000, DSPE-PEG-2000, and Transferrin (Tf) dissolved in  $\text{D}_2\text{O}$ .

**Table S1.** The EXAFS fitting result for analyzing the shell structure of AuCDs of Au-C and Au-Cl bonding value.

Samples	Shell	R(Å)	CN	$\sigma^2$	$R_f$
AuCDs	Au-C	1.93(1)	0.8(5)	0.0023	0.00635
	Au-Cl	2.27(2)	1.2(6)	0.0007	0.00635
<b>Fitting range: <math>3.1 \leq k \text{ (/Å)} \leq 9.9</math> and <math>1.0 \leq R \text{ (Å)} \leq 3.0</math></b>					

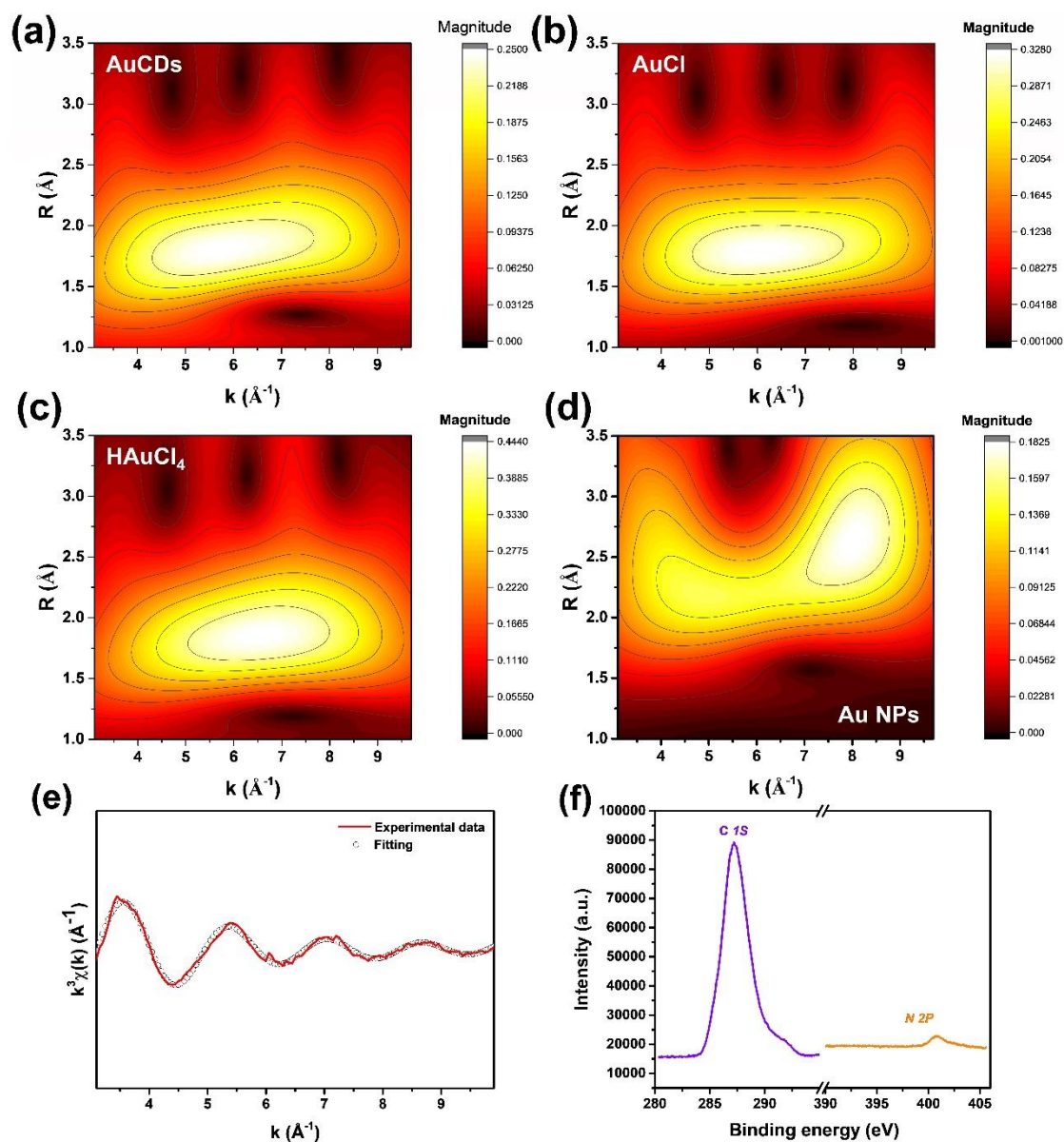


**Fig. S4.** The wavelets diagram of (a) AuCDs, (b) AuCl, (c) HAuCl<sub>4</sub>, and (d) AuNPs demonstrate the difference between the single-atom gold phase and gold clusters. (e) The EXAFS K-space fitting curve. (f) The XPS spectra of CDs.

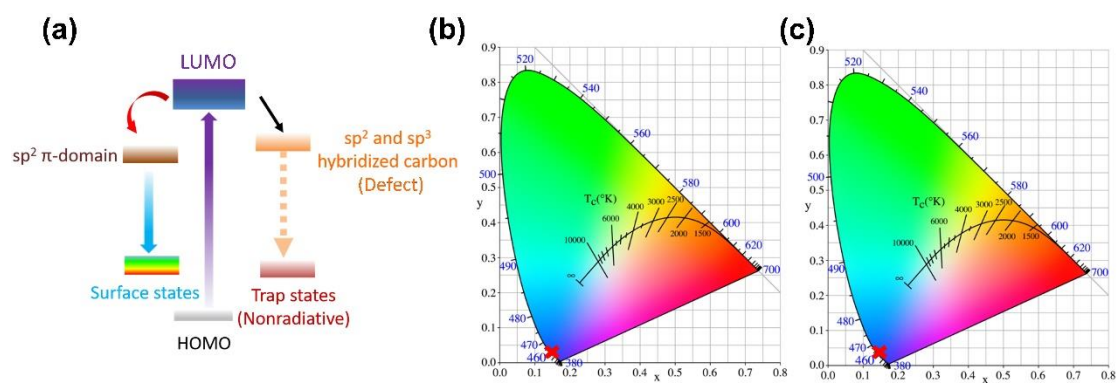


**Fig. S5.** Optical routes and the location of colors of CDs and AuCDs. (a) The emission pathway of CDs. The position in CIE images of (b) CDs and (c) AuCDs.

**Table S2.** The lifetimes result from CDs and AuCDs.

	$A_1$	$A_2$	$\tau_1$ (ns)	$\tau_2$ (ns)
<b>CDs</b>	29576.15	1079.11	$1.33 \pm 0.03$	$5.96 \pm 0.13$
<b>AuCDs</b>	24787.91	842.53	$1.40 \pm 0.03$	$6.15 \pm 0.16$

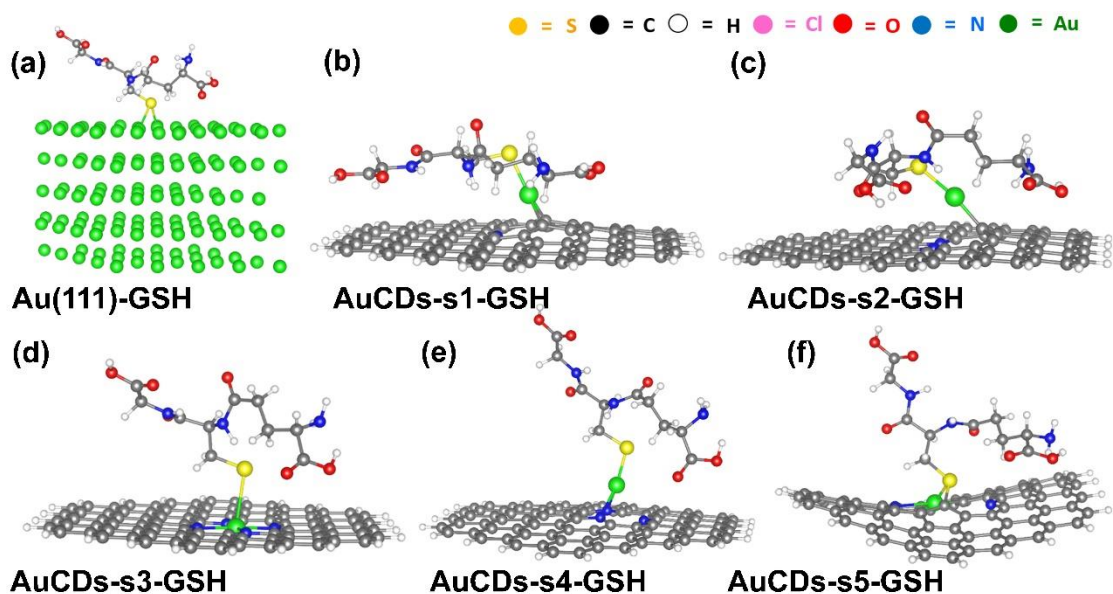


**Fig. S6.** Theoretical calculations are performed to investigate the possible ways of gold-GSH structures through the DFT calculation. (a) Gold nanoparticles. (b-f) AuCDs SAN has different opportunities for binding ways to connect the GSH.

**Table S3.** The potential absorption energy of AuCDs.

Samples	$E_{\text{catalyst}}$ (eV)	$E_{\text{GSH}}$ (eV)	$E_{\text{H}_2}$ (eV)	$E_{\text{complex}}$ (eV)	$E_{\text{adsorption}}$ (eV)
Au(111)	-452.903	-224.167	-6.760	-675.366	-1.68
AuCDs-s1	-955.718			-1179.112	-2.61
AuCDs-s2	-955.676			-1178.661	-2.20
AuCDs-s3	-946.952			-1167.548	0.19
AuCDs-s4	-955.381			-1177.781	-1.61
AuCDs-s5	-915.991			-1138.467	-1.69

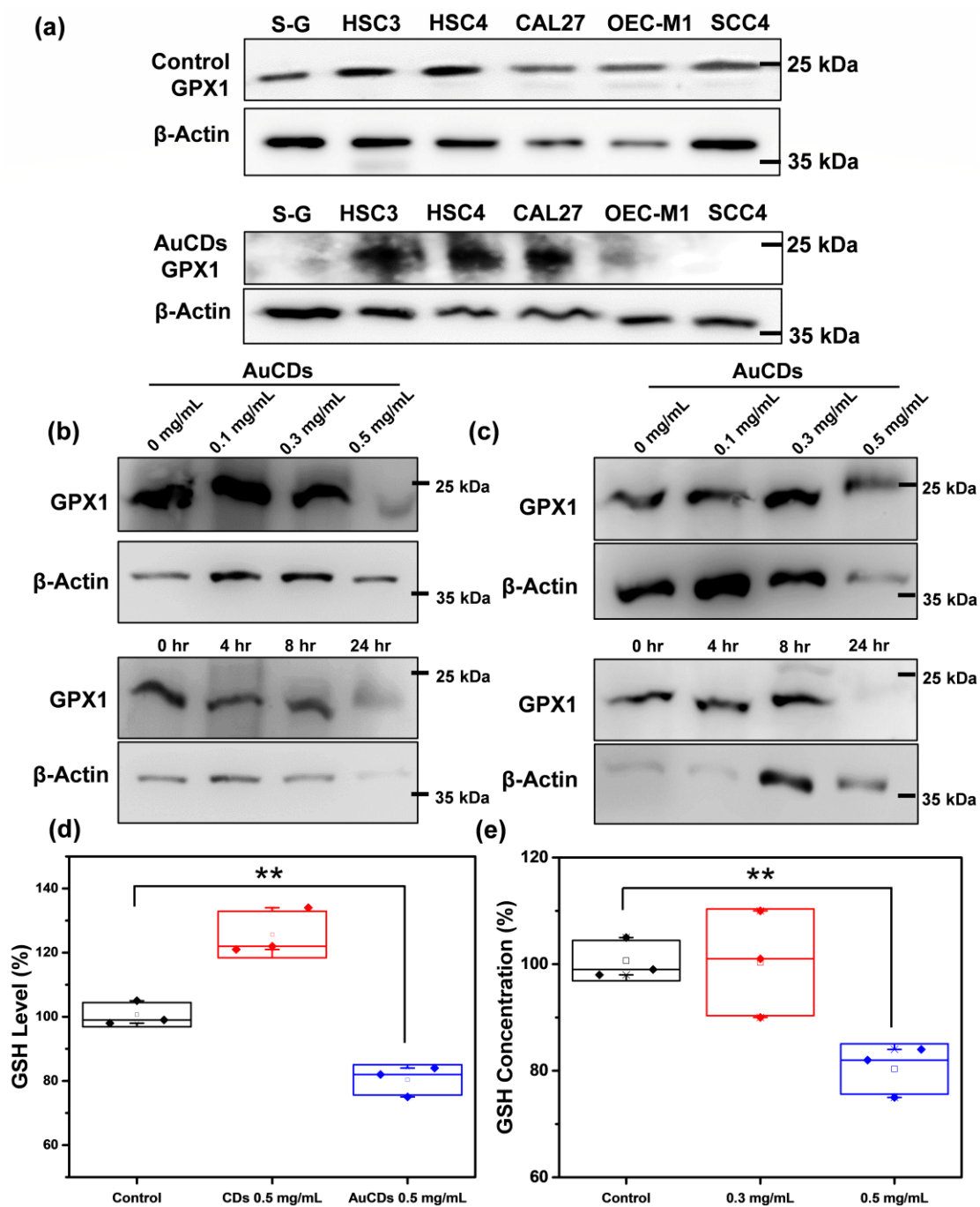


**Fig. S7.** The GSH test conditions were calibrated, and AuCDs SAN was compared with commercially available gold nanoparticle products for catalytic effect. (a) Absorption spectra of GSH at different concentrations. (b) Amplify the absorption spectrum of the most dominant peak (400-500 nm). (c) Corrected regression line of GSH. (d) GSH catalytic testing of AuCDs SAN with commercial gold nanoparticles. P values were calculated by ANOVA (\*\*P < 0.01).

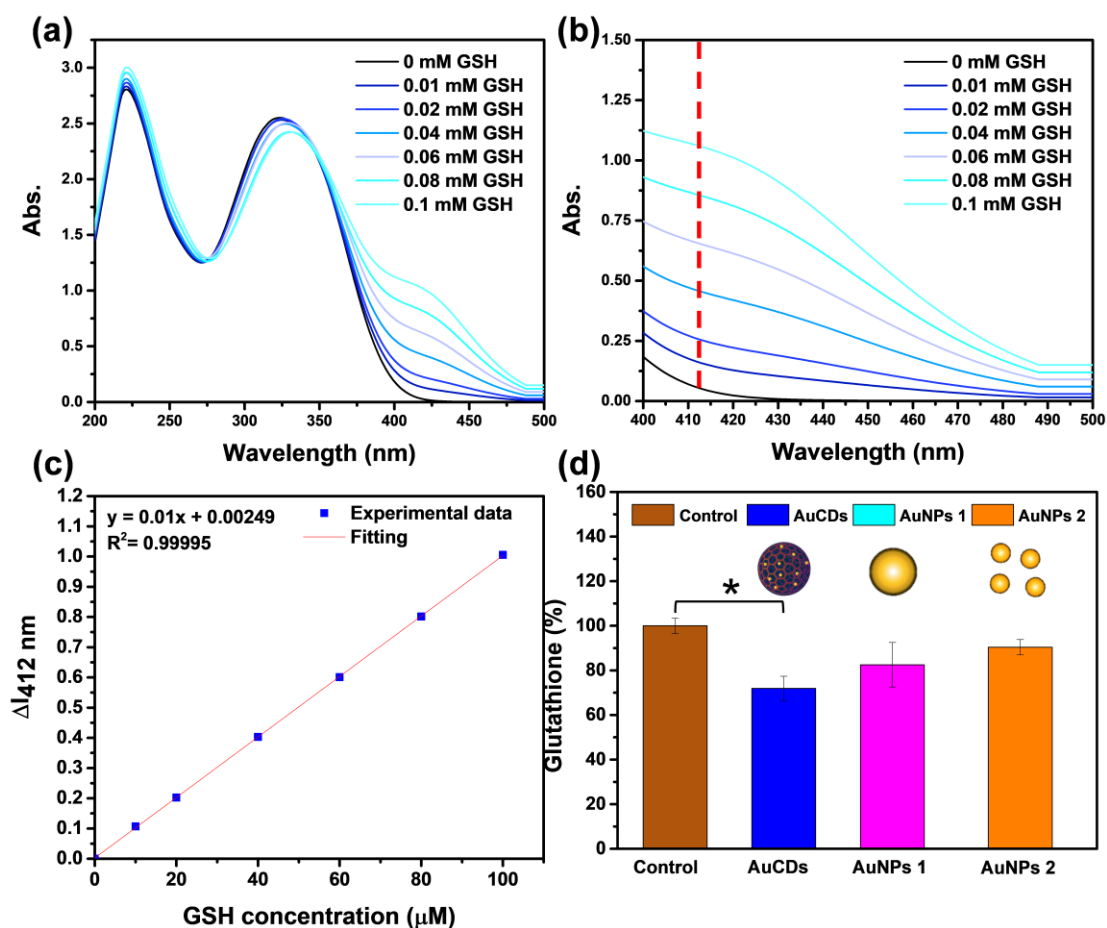


**Fig. S8.** The GSH test conditions were calibrated, and AuCDs SAN was compared with commercially available gold nanoparticle products for catalytic effect. (a) Absorption spectra of GSH at different concentrations. (b) Amplify the absorption spectrum of the most dominant peak (400-500 nm). (c) Corrected regression line of GSH. (d) GSH catalytic testing of AuCDs SAN with commercial gold nanoparticles. P values were calculated by ANOVA (\*\*P < 0.05).

**Table S4.** The absorbance values of GSH calibration curve.

Conc. ( $\mu\text{M}$ )	0	10	20	40	60	80	100
Abs.	0.057	0.16	0.26	0.46	0.66	0.86	1.06
Abs. Variation	0	0.11	0.20	0.40	0.6	0.8	1.01

**Table S5.** List the expression of GPX1 to the candidates of HNSCC with the database, Cancer Cell Line Encyclopedia (CCLE).

<i>Cell lines</i>	<i>State</i>	<i>GPX1 expression</i>
<b>HSC3</b>	<b>UPPER</b>	<b>5.839852</b>
SCC15	UPPER	5.793269
PECAPJ49	UPPER	5.719479
PECAPJ15	UPPER	5.677913
<b>HSC4</b>	<b>UPPER</b>	<b>5.647385</b>
PECAPJ34CLONEC12	UPPER	5.625529
PECAPJ41CLONED2	UPPER	5.541516
BICR31	UPPER	5.473337
BHY	UPPER	5.446422
BICR6	UPPER	5.418883
YD10B	UPPER	5.415339
CAL33	UPPER	5.370031
FADU	UPPER	5.354322
SNU1066	UPPER	5.336297
SCC25	UPPER	5.310704
SCC9	UPPER	5.146211
BICR56	UPPER	5.018539
BICR22	UPPER	4.852329
<b>OEC-M1</b>	<b>UPPER</b>	<b>4.828969</b>
<b>SCC4</b>	<b>UPPER</b>	<b>4.652564</b>
<b>CAL27</b>	<b>UPPER</b>	<b>4.63424</b>
BICR18	UPPER	4.541249

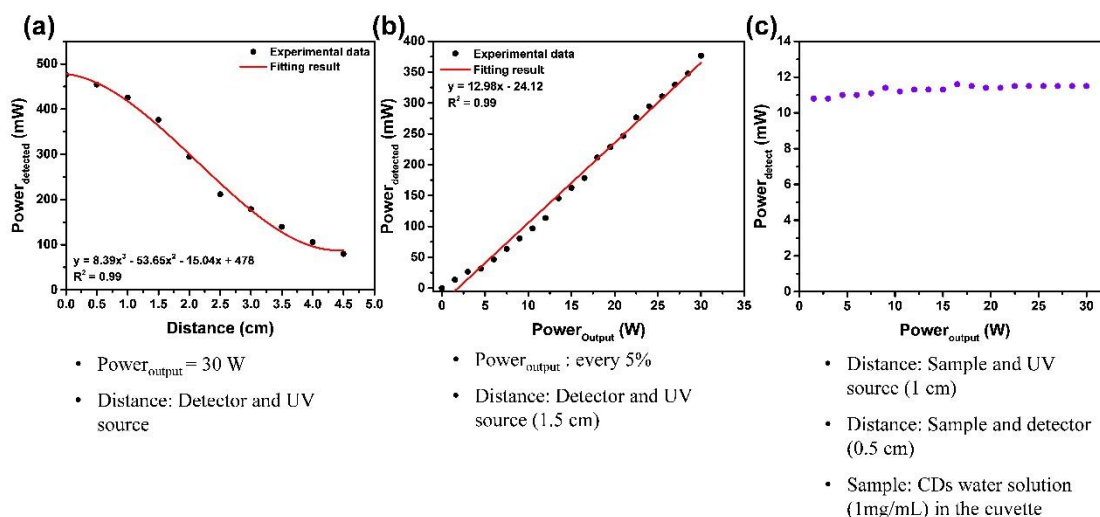


**Fig. S9.** The calibrations of the UV laser light source are completed before experiments. (a) Measurement of the power depends on different distances. (b) Measurement of the linear power curve depends on the additional power Walt of UV laser light. (c) The measure of the stability of the UV light source. The calibration figures were separated into three parts. First, the output power was fixed at 30 W and measured the relation between distance and detected light source. Secondly, the space was set as 1.5 cm. The data of detected power was collected with varied output power. In addition, the CDs solution was put between the detector and the light source, and the distance between the CDs and the light source was 1 cm. The data of detected power was collected with varied output power.

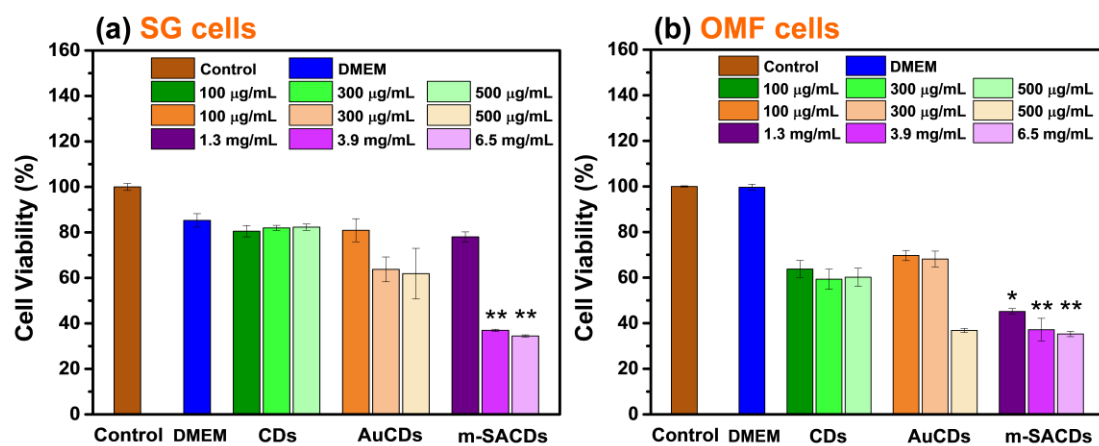


**Fig. S10.** The cell viability analysis of control, CDs, AuCDs, and m-SACDs groups with (a) SG and (b) OMF normal oral cell line. P values were calculated by ANOVA (\* $P < 0.05$  and \*\* $P < 0.01$ ).

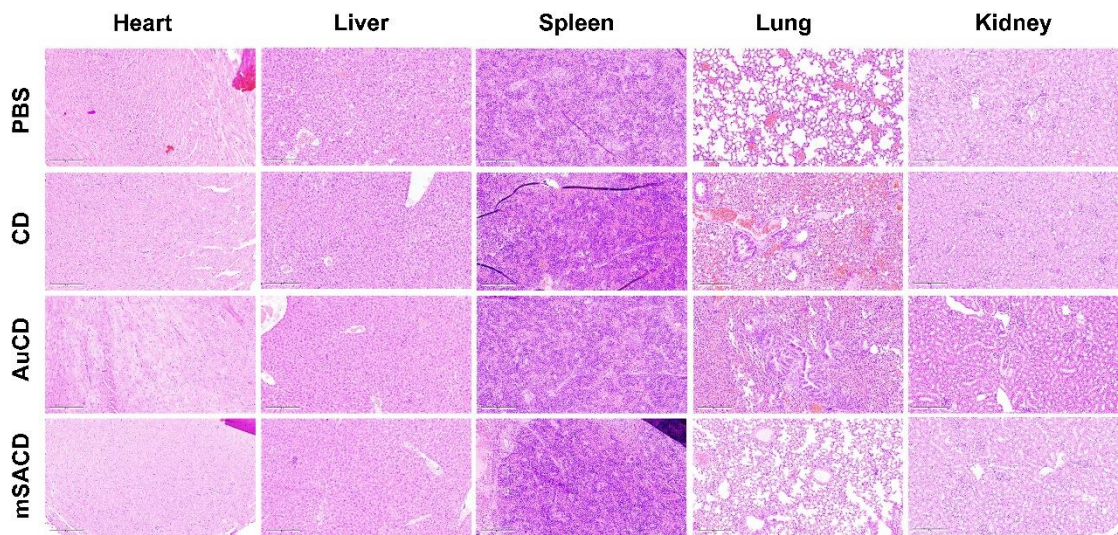


**Fig. S11.** The H&E mice tissue staining of the heart, liver, spleen, lung, and kidney with the control and experimental groups.

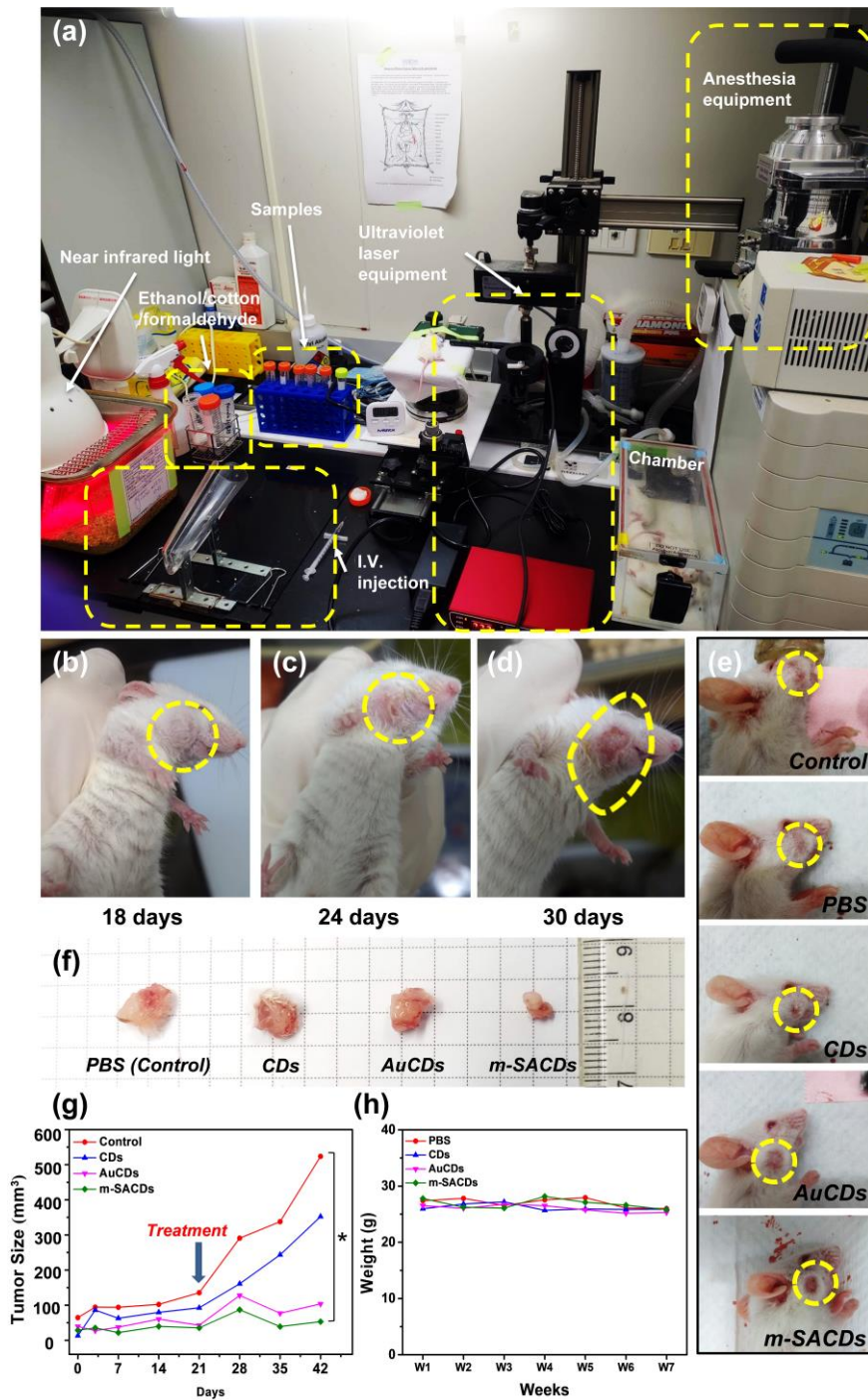


**Fig. S12.** Actual imaging changes of HNSCC tumors in treated mouse oral tissues and *in vivo* treatment test of SCC4 cell line. (a) A realistic picture of drug I.V. administration and light therapy in mice. (b-d) The necrosis of OEEM-1 tumor under the m-SACDs treatment with the irradiation of UV light for 18, 24, and 30 days. (e) Comparing different experimental groups demonstrates the tumor's surface change for 21 days. (f) The visual image of the SCC4 tumor, (g) the tumor growth curves of SCC4 tumors, and (h) the weight of mice after treatment with four different groups. P values were calculated by ANOVA (\*P < 0.05).